An Objective Satellite-Based Tropical Cyclone Size Climatology

JOHN A. KNAFF

Regional and Mesoscale Meteorology Branch, NOAA/NESDIS, Fort Collins, Colorado

SCOTT P. LONGMORE

Cooperative Institute for Research in the Atmosphere, Colorado State University, Fort Collins, Colorado

DEBRA A. MOLENAR

Regional and Mesoscale Meteorology Branch, NOAA/NESDIS, Fort Collins, Colorado

(Manuscript received 8 February 2013, in final form 16 August 2013)

ABSTRACT

Storm-centered infrared (IR) imagery of tropical cyclones (TCs) is related to the 850-hPa mean tangential wind at a radius of 500 km (V500) calculated from 6-hourly global numerical analyses for North Atlantic and eastern North Pacific TCs for 1995–2011. V500 estimates are scaled using the climatological vortex decay rate beyond 500 km to estimate the radius of 5 kt (1 kt = 0.514 m s^{-1}) winds (R5) or TC size. A much larger historical record of TC-centered IR imagery (1978–2011) is then used to estimate TC sizes and form a global TC size climatology. The basin-specific distributions of TC size reveal that, among other things, the eastern North Pacific TC basins have the smallest while western North Pacific have the largest TC size distributions. The life cycle of TC sizes with respect to maximum intensity shows that TC growth characteristics are different among the individual TC basins, with the North Atlantic composites showing continued growth after maximum intensity. Small TCs are generally located at lower latitudes, westward steering, and preferred in seasons when environmental low-level vorticity is suppressed. Large TCs are generally located at higher latitudes, poleward steering, and preferred in enhanced low-level vorticity environments. Postmaximum intensity growth of TCs occurs in regions associated with enhanced baroclinicity and TC recurvature, while those that do not grow much are associated with west movement, erratic storm tracks, and landfall at or near the time of maximum intensity. With respect to climate change, no significant long-term trends are found in the dataset of TC size.

1. Introduction

Tropical cyclones (TCs) occur in many regions around the globe including the North Atlantic, eastern North Pacific, western North Pacific, north Indian Ocean, and Southern Hemisphere. There are many agencies that issue advisories, warnings, and forecasts of these systems. The typical advisory contains information about individual TC location, movement, intensity (in terms of maximum wind speed, and minimum sea level pressure), and in many cases radii of significant wind speeds (e.g., the extent of gale-force wind speeds). Much of the focus of TC research has concentrated on motion and intensity, but it is the TC size in terms of wind field that often determines potential tropical cyclone impacts (e.g., Powell and Reinhold 2007; Houston et al. 1999; Irish et al. 2008) and areal coverage and distribution of rainfall (e.g., Kidder et al. 2005; Matyas 2010). In this paper we will concentrate of variations of TC size.

Past studies of TC wind structure (Weatherford and Gray 1988; Chan and Chan 2012) have shown that the intensity (i.e., the maximum wind speed) is not strongly related to the strength of the wind field beyond a distance of 111 km (1° latitude) from the center but the storm strength [i.e., the average wind speeds between 111 and 278 km (1° and 2.5° latitude) from the center as defined by Weatherford and Gray (1988) are strongly related and positively correlated with the maximum radial extent of 34-kt (1 kt = 0.514 m s^{-1}) wind speeds (R34)]. This implies simply that knowing the TC intensity is not enough information to determine the TC's

Corresponding author address: John Knaff, NOAA/NESDIS, CIRA, Campus Delivery 1375, Colorado State University, Fort Collins, CO 80523-1375.
E-mail: john.knaff@noaa.gov

DOI: 10.1175/JCLI-D-13-00096.1

wind field structure. TC size in terms of R34 also tends to increase during extratropical transition (Brand and Guard 1979; Evans and Hart 2008). Low-level TC kinetic energy (within 200 km) also tends to increase when TCs encounter moderate to strong vertical wind shear, they experience synoptic-scale warm air advection, and/or when TCs experience eyewall replacement cycles (Maclay et al. 2008). Others have documented the small-sized nature of TCs that form close the equator (Brunt 1969) and in the eastern North Pacific (Knaff et al. 2007) and midget typhoons that occur at subtropical latitudes (Arakawa 1952; Brand 1972; Harr et al. 1996) in terms of R34.

Similar to R34, the radius of the outermost closed isobar (ROCI) has also been used as a TC size metric. This is because ROCI is well related to the tangential wind speed profile of hurricanes and operational estimates of ROCI were and are routinely made available from many archives. When the ROCI is large, the TC's tangential wind speed profile is broader; when ROCI is smaller, the tangential wind speed profile is more compact (Merrill 1984). Others have shown that the initial size of the wind and/or pressure fields is often roughly maintained as TCs intensify (Cocks and Gray 2002; Dean et al. 2009; Chavas and Emanuel 2010; Lee et al. 2010), suggesting that initial ROCI is important to determining TC structure at later times.

Most past studies of TC structure variation, however, have been conducted in the western North Pacific or North Atlantic TC basins and have used differing definitions of TC size based mostly upon a mixture of ROCI and/or R34. In many of these studies, the number of years and cases was limited by short data records. The studies of Merrill (1984), Chan and Chan (2012), and Lee et al. (2010) are among the most comprehensive studies to date. Merrill (1984) used ROCI as a size metric 1957–77 (Atlantic) and 1961–69 (western North Pacific), and both Chan and Chan (2012) and Lee et al. (2010) used Quick Scatterometer (QuikSCAT) surface wind speed estimates for 1999–2009 and 2000–05, respectively. These latter studies use wind speed thresholds that are close to 34 kt as a size metric. Unfortunately, to date no global TC size climatology has been created.

Past studies have nearly exclusively relied upon the R34 and ROCI as size metrics and, while it is has been shown that these two metrics are related, they are not the same. These measures also have a number of shortcomings that make climatological studies and interbasin comparisons difficult. In most cases R34 and ROCI are subjective estimates made from the available data and are method dependent. Admittedly, objective R34 estimates are possible using scatterometry, but those records are relatively short (since the late 1990s). To further complicate matters, the specific methods used to estimate ROCI and R34 have varied over the years and such changes are not well documented. Furthermore, the use of the 34-kt wind speed threshold precludes studies of weaker TCs with maximum wind speeds below this threshold. Asymmetries in the wind field also make estimating a mean R34 difficult as discussed in Demuth et al. (2006). Finally, the ROCI, besides being subjective and method dependent, is also a function of the pressure field and environment in which a TC is embedded. For instance, the ROCI would be infinite for a TC vortex with no environmental flow, but ROCI would also shrink solely because of accelerations in the mean flow–motion.

For these reasons, we endeavor to create a TC size metric that can be applied in a uniform manner globally over a long period of record to assess the climatology of TC size and compare to the previous studies. We also define TC size as the radius at which the TC influence on the near-surface wind field is indistinguishable from that of a climatological environment, much as Dean et al. (2009) and Chavas and Emanuel (2010) did. To do this we employ historical records of TC location, digital infrared (IR) imagery, and large-scale environmental diagnostics of TCs to develop an algorithm for TC size and apply it to the global TC records. The following sections discuss the details of our data, methods, and results.

2. Data description

a. Infrared satellite information

For this study, we use the brightness temperatures T_b from 3-hourly storm-centered IR imagery from the global constellation of geostationary satellites. The sources of these images come from two archives. The first is the Hurricane Satellite data, version 3 (HURSAT v3; Knapp and Kossin 2007). This dataset provides 8 km × 8 km Mercator images that contain 3-hourly storm-centered IR T_b [with window ($\sim$11 μm) wavelengths] that are centered on global TCs starting in 1978 and ending in 2006. The second IR image archive comes from the Cooperative Institute for Research in the Atmosphere (CIRA) tropical cyclone IR image archive (referred to as the CIRA IR archive), which contains IR window observations of TCs that have been remapped to 4 km × 4 km Mercator projection from various geostationary satellite platforms as described in Zehr and Knaff (2007). The CIRA IR archive, which has a higher temporal and spatial resolution, is used here to extend HURSAT v3 through 2011 at the same 3-hourly temporal resolution.

b. TC track and intensity information

The storm location and intensity information used in this study comes from two sources. The first, for the period 1978–2006 (i.e., for the HURSAT cases), is

contained in the HURSAT data files. That information is provided by the International Best Track and Archive for Climate Stewardship (IBTrACS; Knapp et al. 2010) The second source that is used to estimate storm location and intensity for the 2007–11 period (i.e., for the CIRA IR archive cases) is provided by the databases of the Automated Tropical Cyclone Forecast (ATCF; Sampson and Schrader 2000) system. These contain the final best track information produced by the National Hurricane Center (NHC), the Central Pacific Hurricane Center, and the Joint Typhoon Warning Center (JTWC). For this study, we will use the native ATCF units for TC intensity, which are knots. Cubic spline interpolation is used to obtain estimates of the 3-hourly positions and intensities that are used in this study. We will also examine the TC formation basins that are contained in the ATCF database for this study. These basins include the North Atlantic, eastern North Pacific, central Pacific, western North Pacific, north Indian Ocean, and Southern Hemisphere. The few TCs that form in the central Pacific are combined with those that form in the eastern North Pacific.

c. *Large-scale TC diagnostics*

For algorithm development, we use the large-scale diagnostic fields of the Statistical Hurricane Intensity Predictions Scheme (SHIPS) and the Logistic Growth Equation Model (DeMaria et al. 2005; DeMaria 2009). Specifically, we use the estimates of 1) azimuthal mean tangential wind at 850 hPa at the 500-km radius and 2) the vorticity at 850 hPa averaged out to a 1000-km radius. Both of these quantities are calculated from Global Forecast System (GFS)-based model analyses [operational analyses for 2000–11 and National Centers for Environmental Prediction–National Center for Atmospheric Research (NCEP–NCAR) reanalyses (Kalnay et al. 1996) for 1995–99]. The 850-hPa azimuthally averaged tangential wind at 500 km is the quantity we use to train our algorithm. The 850-hPa vorticity at 1000 km is used to estimate the azimuthally averaged tangential wind at 1000 km, which is then used for the climatological scaling of our estimates of TC size. Specific details of how these are used to create an objective measure of TC size are described in the next section.

3. Methods and scaling

a. *Processing IR images*

The 3-hourly T_b values were analyzed to storm-centered polar grids with 4-km radial spacing and 10° azimuthal spacing. The domain of these analyses is 602 km in radius. The storm centers provided in the HURSAT dataset are used for these polar analyses of HURSAT imagery. For the CIRA IR archive, storm centers are estimated via interpolation from the nominal times of the images and the 6-hourly positions in the best track. The polar analyses are created using the variational analysis technique described in Mueller et al. (2006), but smoothing constraints are chosen so that the half-power wavelengths of the filter were 10 km in radius and 22.5° in azimuth. This procedure provides a uniform way of comparing and using the information from the HURSAT and CIRA IR archive and allows for other, more complicated analyses in the future.

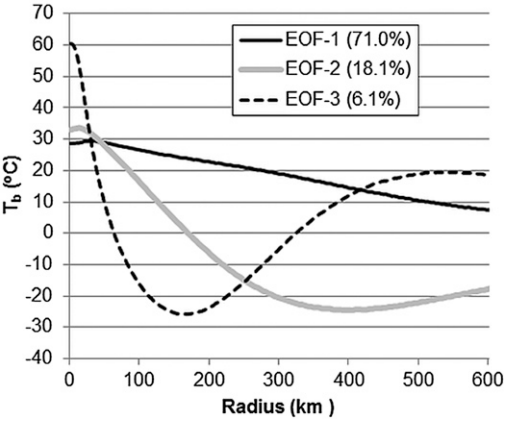

FIG. 1. Leading modes of variability or EOFs of the 6-hourly mean azimuth-averaged profiles of T_b. The percent of the variance explained by each EOF is shown in parentheses.

To significantly simplify the problem of relating IR imagery to TC structure, we then take azimuthal averages of the resulting polar T_b analyses, standardize those profiles at each radius (removing the sample radial mean and dividing by the sample radial standard deviation), and then perform a principal component analysis. Figure 1 shows the leading modes of variability or empirical orthogonal functions (EOFs) along with the percent variance explained by each mode. EOF 1 is associated with the mean cloud top temperatures (radial wavenumber zero). EOFs 2 and 3 are related to the radial structure of T_b as radial wavenumber 1 and 2, respectively. These first three EOFs explain more than 95% of the azimuthally averaged T_b variance. In essence, this procedure simplifies the problem by reducing 151 azimuthal averages to three principal variables that explain the majority of the radial structure of T_b. Principal components are then created for each 3-hourly image in our combined HURSAT and CIRA IR archive dataset.

b. *TC size algorithm development*

For this study, we use the azimuthally averaged 850-hPa tangential wind at the radius of 500 km as a proxy for TC

size. There are several reasons for using this metric instead of the traditional metrics of ROCI or R34. The first justification is that the traditional metrics have significant shortcomings, as described in the introduction. Another justification is that the mean tangential wind at a fixed radius is related to both the circulation and the average vorticity via Stokes theorem. This definition also allows the application of Kelvin's circulation theorem whereby the absolute circulation is quasi conserved in the generally quasi-barotropic tropical atmosphere and outer regions of the TC. The Stokes theorem also implies that the tangential winds decrease as the radius–area increase. This relationship has been shown observationally in TCs by several authors (e.g., Weatherford and Gray 1988; Cocks and Gray 2002) and is the basis of parametric vortex models (Depperman 1947; Holland 1980). Furthermore, if the TC maintains a constant angular momentum, the mean tangential wind at 1000 km should be close to a quarter of its value at 500 km. This also implies that there is some radius where the circulation is close to the background flow, a relationship we later use for scaling. The 850-hPa level is used as an estimate for the winds above the frictional boundary layer. It is also noteworthy that a similar strategy was successfully used to estimate TC size and provide improved wind–pressure relationships (Knaff and Zehr 2007).

We are also confident the current global models and reanalyses estimate the 850-hPa mean tangential wind at a radius of 500 km (V500) accurately enough that it can be used for this type of algorithm development. Indirect evidence that similar analysis-derived diagnostics do a good job in estimating the TC environment come from the success of a number of statistical TC applications that have been trained using such diagnostics. A few examples of such applications include the statistical hurricane intensity prediction scheme (DeMaria et al. 2005), the logistic growth equation model (DeMaria 2009), the rapid intensification index (Kaplan et al. 2010), the tropical cyclone formation product (Schumacher et al. 2009), and tropical cyclone wind–pressure relationships (Knaff and Zehr 2007). For our study we use the NCEP reanalyses and operational GFS analyses and accept that these have known shortcomings[1] and that the type and quality of data used in data assimilation has changed over time.

Since we propose to relate symmetric features in IR imagery to TC size, we also want the TC size metric chosen to be well matched with the observed TC convective structure. Frank (1977) found a ''moat'' region where moderate subsidence occurs below 400 hPa in rawinsonde composites and where convection is suppressed. Frank (1977) also showed that, while the convective portion of the storm is located radially inside this moat region, the storm-induced tangential winds commonly extended beyond the 1550-km domain of his analysis (i.e., the wind field is larger than the convective field). The moat is typically located at a radius of between 4° and 6° latitude but varies from case to case. Previous studies have also shown that the areal extent of convection surrounding TCs is related to the areal extent of the TC's wind field (Shoemaker 1989; Cocks 1997; Cocks and Gray 2002; Mueller et al. 2006; Kossin et al. 2007; Lee et al. 2010). It is this relationship between the areal extent of the TC's cloud–IR field and the areal extent of the TC's wind field we would like to exploit. Thus, the TC size metric we proposed is both located at the same scale as the typical convection-suppressed TC moat region and can be easily quantified by structures in IR imagery.

To create an objective IR-based estimate of TC size, we use the V500 from the SHIPS large-scale diagnostic files as the dependent variable of a multiple linear regression. The potential predictors for this regression are the sine of the absolute value of storm latitude and the normalized principal components of the azimuthally averaged radial profiles of T_b from the center of the TC out to a radius of 602 km (i.e., associated with the EOFs shown in Fig. 1). Previous studies have shown that these principal components can explain much of the symmetric TC vortex structure (Mueller et al. 2006; Kossin et al. 2007), further justifying this approach. A 6-hourly subset of the Atlantic- and east Pacific–dependent sample of 1995–2011 that contained data from the CIRA IR archive was used for initial algorithm development. The resulting multiple regression equation explains 29% of the variance of observed V500 and has a root-mean-square error of 2.9 m s^{-1}. The resulting regression equation is

$$\mathrm{V500} = 2.488 + 11.478 \times \sin|\varphi| - 1.350 \times \mathrm{PC1} + 0.912 \times \mathrm{PC2} + 0.319 \times \mathrm{PC3}. \quad (1)$$

In (1), φ is latitude and PC1, PC2, and PC3 are the normalized principal components. Each predictor is statistically significant at the 99% level using a two-tailed Student's t test. The positive coefficient associated with the latitude term implies that storms grow as they move poleward. Two likely reasons are that TCs import more angular momentum than needed to maintain their current intensity and size and/or that baroclinicity, which increases as the TC moves poleward, promote TC

[1] The most severe shortcomings in the NCEP–NCAR reanalyses with respect to downscaling tropical cyclone features are found prior to 1980 when the satellite data input dramatically changed (Emanuel 2010).

TABLE 1. General statistics related to the V500 and R5 estimates. V500 is estimated by (1) and R5 is estimated by (2). Units for V500 and R5 are meters per second and DDLAT, respectively.

	No. of cases	Mean	Standard deviation	Median	First quartile	Third quartile
V500 ($m\,s^{-1}$)	122 989	6.56	2.09	6.61	5.09	8.08
R5 (DDLAT)	122 989	11.00	3.36	11.08	8.63	13.43

growth. These mechanisms are consistent with Merrill's (1984) findings. This term also implicitly includes effects related to satellite viewing angle, and cloud top T_b increases with latitude. The negative coefficient on PC1 implies TCs with colder cloud shields (r = 0–600 km) tend to be larger. The positive coefficients with PC2 and PC3 are also consistent, suggesting colder cloud tops from r = 200–600 km and from r = 70–300 km, respectively, are related to larger TCs (see Fig. 1). Table 1 provides the statistics associated with V500 estimated by (1) for the entire 3-hourly dataset for 1978–2011.

Since TC size implies units of distance or area, we scale the estimated V500 that comes from (1) using the climatological (1995–2011) mean linear relationship between the azimuthally averaged tangential wind at 500 km (V500c) and at 1000 km (V1000c). V1000c is derived from the average (r = 0–1000 km) vorticity ζ_{1000} using this relationship V1000c = $r \times \zeta_{1000}$, where r is the radius. Using the slope of this relationship and an estimate of V500 [i.e., from (1)], the radius where the mean tangential wind at 850 hPa is 5 kt (R5) is found. For our study, a 5-kt tangential wind at 850 hPa is assumed to be essentially the same as the background flow. So, in the simplest terms, R5 is the radius of where the TC wind field is indistinguishable from the background flow in a climatological environment. We note here that both Dean et al. (2009) and Chavas and Emanuel (2010) took a different approach.

The relationship between V500 and R5 is provided by

$$\mathrm{R5} = \left[\overline{\mathrm{R5}} + (\mathrm{V500} - \mathrm{V500c})\frac{500}{\mathrm{V500c} - \mathrm{V1000c}}\right], \qquad (2)$$

where the climatological mean values of R5, V500, and V1000 are $\overline{\mathrm{R5}}$ = 952 km, V500c = 5.05 $m\,s^{-1}$, and V1000c = 2.23 $m\,s^{-1}$, respectively, and V500 is estimated using (1). The values of R5 are consistent with the TC composites of Frank (1977) where the tangential wind associated with an average TC extended beyond his 1554-km analysis domain. To make the units more manageable and to allow better comparison with historical work on this subject, we will present R5 in units of distance in terms degrees latitude (DDLAT; 1 DDLAT = 111.11 km) for the remainder of the paper. It is noteworthy that over 99% of R5 estimates are less than 21° latitude (2330 km) but greater than 4° latitude (440 km). Finally, the error characteristics of R5 are linearly dependent on the errors associated with the estimation of V500. Table 1 provides the statistics associated with R5 estimated by (2) for the entire 3-hourly dataset of 1978–2011.

A reasonable question to ask is how R5 (and/or V500) is related to R34 (or gale force) winds. Using the same 6-hourly developmental dataset used for algorithm development, we relate the R5 estimates to the azimuthal average of the nonzero quadrant values of the operational 34-kt wind speed radii (R34) from the NHC. As discussed in Demuth et al. (2006), excluding the quadrants with zero wind radii from azimuthal averages removes noise associated with cases where the maximum wind speed is close to the 34-, 50-, or 64-kt wind radii thresholds. In such cases, wind radii in some quadrants can rapidly fluctuate between zero and nonzero values as a function of time. For the combined eastern North Pacific and North Atlantic sample, R5 explains 30% of the variance of R34. However, the region where gale-force winds are typically found in a TC is located between the core region of the storm, which is best related to intensity, and the outer regions of the TC where R5 provides an estimate of the size of the wind field. Therefore it might be expected that R34 is both a function of intensity in terms of maximum wind speed $V_{\max}$ and R5–TC size. This is indeed the case. When R5 and $V_{\max}$ are used in a multiple linear regression, they explain 38% of the R34 variance. The regression equation, which is best related to TCs with symmetric wind structures, is

$$\underline{\mathrm{R34}} = -98.63 + 1.33V_{\max} + 28.19 \times \mathrm{R5}, \qquad (3)$$

where R34 has units of kilometers, $V_{\max}$ has units of knots, and R5 has units of DDLAT. The relationship in (3) has root-mean-square errors of 74 km and mean absolute errors of 55 km. These errors are similar to those presented in Knaff et al. (2011) but much larger than the results of Demuth et al. (2006). The 38% of the variance explained is also similar to results comparing scatterometer-based R34 estimates with those of the JTWC in Lee et al. (2010). This demonstrates that R5 is related to the R34 TC size metric.

The significant scatter between the R34 and the R34 predicted using the multiple regression (3) is somewhat

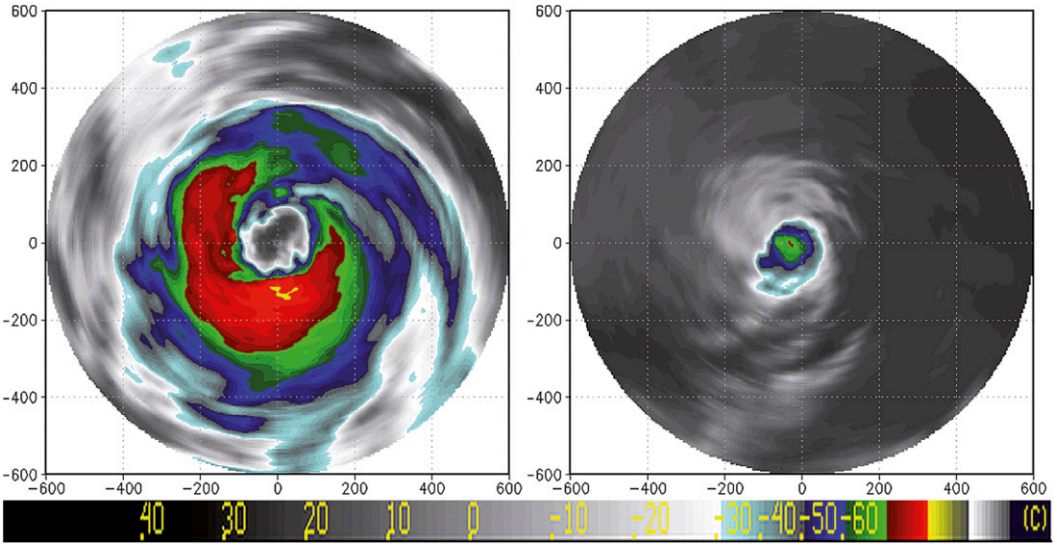

FIG. 2. IR images of (left)Typhoon Abe (1990) located at 25.2°N, 124.8°E with an intensity of 90 kt at 0000 UTC 30 Aug 1990 and (right) Hurricane Kay (1998) located at 16.0°N, 123.8°W with an intensity of 65 kt at 1800 UTC 13 Oct 1998. These images also had PC1 values of −1.07 and 0.99, PC2 values of 2.83 and −2.31, and PC3 values of 2.09 and −2.62 for Typhoon Abe and Hurricane Kay, respectively. These represent the largest and smallest hurricane intensity TCs (at their maximum lifetime intensity) in our dataset.

expected as (3) does not account for the variability of TC's environment. This shortcoming highlights an additional but subtle property of the R5 algorithm developed above. The large scatter associated with the regression in (1) is primarily due to the variable environmental conditions in which individual TCs exist. In other words, the observed V500 is due to a TC component and an environmental component. The environmental component, as would be expected, is not related to the symmetric IR depiction of the TC in (1). Furthermore, a climatological environment is used to arrive at estimates of R5 in (2). As a result, V500 estimated by (1) and R5 estimated by (2) are primarily related to variations in TC structure rather than in the TC environment. This is a fortunate property for the R5 algorithm to have as it is actually convenient to minimize the influence of different environments for the purposes of this study.

Finally, to provide the reader an example of how this method applies to individual images, Fig. 2 shows the IR images associated with western North Pacific Typhoon Abe (1990), and eastern North Pacific Hurricane Kay (1998). These two TCs were the largest and smallest hurricane intensity (>64 kt) TCs at the time of maximum lifetime intensity found in our study. The R5 values calculated for these images are 19.8 and 2.7 DDLAT for Typhoon Abe and Hurricane Kay, respectively. The R5 estimates imply that Typhoon Abe is 53 times larger, in terms of area, than Hurricane Kay. Visually, Fig. 2 depicts a situation where the entire cold cloud shield of Kay fits inside the ragged eye of Abe.

4. Results

In this section, we present a basic climatology of R5 as a measure of the TC vortex size. The following subsections will describe the IR image composites of TC size as measured by the R5 metric, interbasin TC size distributions, the mean life cycle of TC size, spatial and seasonal distributions of large and small TCs, the spatial details of where TCs tend to grow the most/least, and finally the interannual trends of TCs size. Hereafter, R5 and TC size will be used interchangeably. In this section, we will also use the following definitions for intensity ranges. To reduce confusion and unnecessary verbosity, TCs will be referred to as tropical depressions, tropical storms, minor hurricanes, and major hurricanes when there intensities are $V_{\max} < 34$ kt, $34 \le V_{\max} < 64$ kt, $64 \le V_{\max} < 96$ kt, and $V_{\max} > 96$ kt, respectively.

a. IR composites of TC size

To provide the reader with a sense of how the R5 metric is related to the structures in IR imagery, composite averages of IR imagery as a function of TC intensity and TC size were computed. Figure 3 shows the average of IR images for small, average, and large-sized TCs, which correspond to the 1σ variations about the distribution of R5 (see Table 1). The number of images

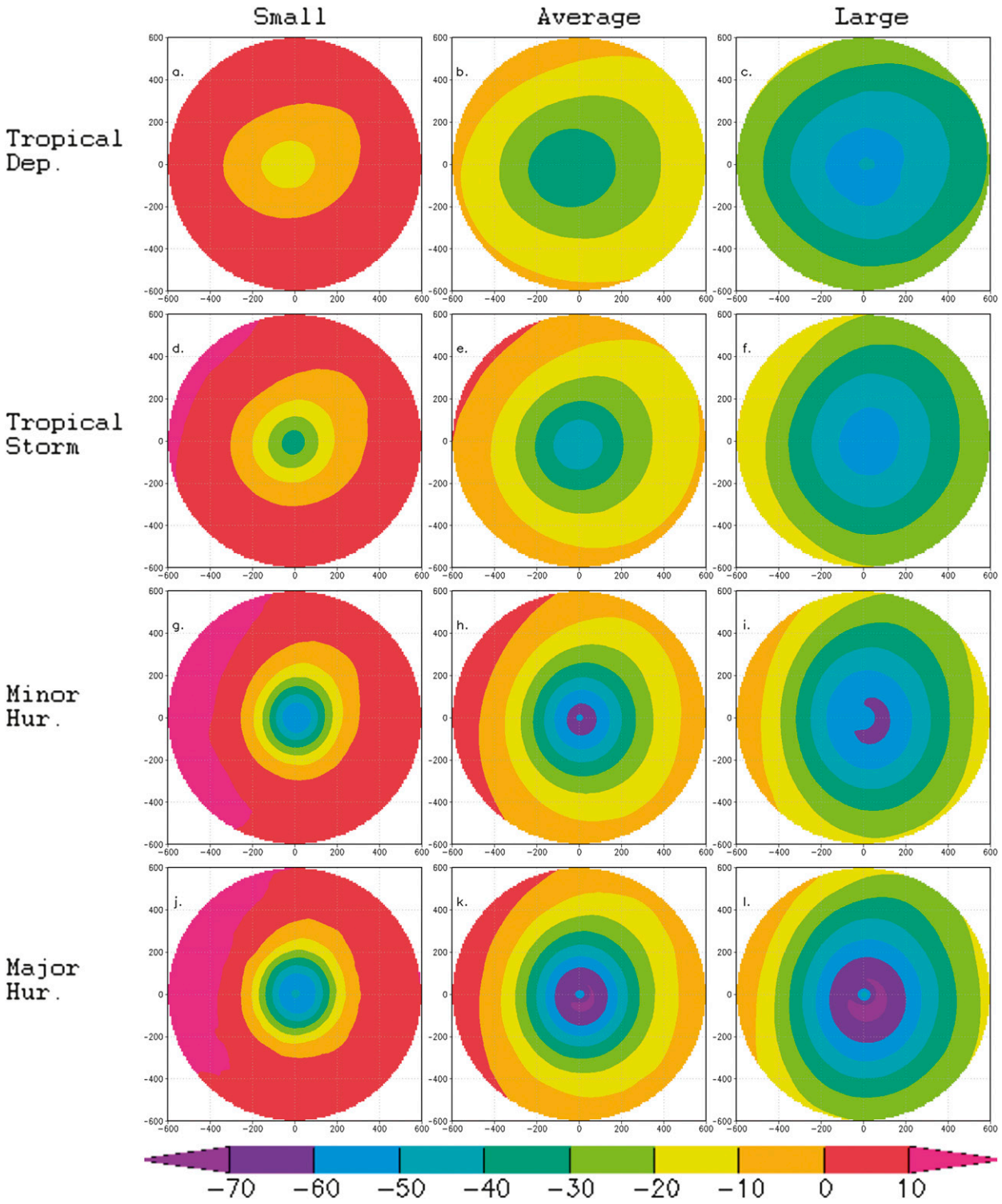

FIG. 3. Composite average T_b for TCs with intensities of (a)–(c) <34 kt, (d)–(f) 34–63 kt, (g)–(i) 64–95 kt, and (j)–(l) >95 kt and R5 sizes of (a),(d),(g),(j) <7.5°, (b),(e),(h),(k) 7.5°–12.45°, and (c),(f),(i),(l) >12.45° latitude. The scale for T_b (°C) is provided at the bottom of the figure. The number of individual images used in each composites is (a) 18 686, (b) 38 667, (c) 4133, (d) 9045, (e) 39 741, (f) 10 127, (g) 1783, (h) 16 394, (i) 9361, (j) 426, (k) 6412, and (l) 6369. Similarly, the mean intensities are (a) 25, (b) 25, (c) 27, (d) 43, (e) 46, (f) 48, (g) 76, (h) 77, (i) 79, (j) 108, (k) 113, and (l) 118 kt. Each panel shows IR T_b values within a 602-km radius.

TABLE 2. List of spatial statistics of the composite T_b images shown in Fig. 2. The number of cases, the spatial mean, and spatial standard deviation σ are provided for each composite image.

	Small composites			Average composites			Large composites		
	No.	Mean	σ	No.	Mean	σ	No.	Mean	σ
Tropical depressions	18 686	1.8	4.8	38 667	−18.3	7.9	4133	−36.0	9.2
Tropical storms	9045	1.1	8.4	39 741	−15.9	10.8	10 127	−31.4	10.9
Minor hurricanes	1783	1.2	13.6	16 394	−16.3	15.6	9361	−30.4	14.7
Major hurricanes	426	0.7	15.2	6412	−18.4	18.4	6469	−34.1	17.0

and mean intensities of each panel are provided in the figure caption. The figure shows that the composite images for tropical depressions (Figs. 3a–c) are fairly symmetrical with the area containing T_b values colder than −10°, −30°, and −50°C being roughly the same for small, average, and large composites, respectively. The large-sized tropical depression composite also contains a central warm spot, but upon closer examination the temperature differences are very small (≤1°C) and are being overemphasized by the choice of contour thresholds. The second row, Figs. 3d–f, shows the images associated with tropical storms. These composite images are similar to those of the tropical depressions, but the range of T_b is larger. The T_b contours in these composites have larger gradients with noticeably colder central features. The next row, Figs. 3g–i, shows the composite images of minor hurricanes. Compared to tropical storms, the range of T_b continues to increase and a slight shrinking of the −10°, −20°, and −30°C contours is evident in the minor hurricane composites as the core region consolidates. A warm feature is only evident in the average-sized composites, but again upon closer examination a central warm feature is evident in all three minor hurricane composites but is not highlighted by the contour interval. The final row, Figs. 3j–l, shows the major hurricanes composite images. In this row there is clear evidence of the existence of the TC eye at all sizes. Again the T_b range in the composites increases from the minor hurricane composites shown in the row above. The small TC composites of both major and minor hurricanes shows generally warmer T_b exist within 100 km of the TC center compared to the average and large composites with corresponding intensity ranges.

A simple way to determine the statistical significance of these composites is to compare the spatial means of the composites. Table 2 provides the number of cases, the spatial mean T_b, and the standard deviation of T_b for each composite. Using the Student's t test, the difference in means of the small, average, and large composites for each intensity bin are significant at the 99% level.

Figure 3 provides the reader a visual reference for the gross variability of IR features explained by the R5 metric. Furthermore, the results provide more confidence that R5 is well related to the size of the cold cloud shield (a proxy for TC size) variations rather than variable environmental conditions. For small- and average-sized TCs the region with $T_b < -20°$ and −10°C appear nearly the same as the TC intensifies from depression to major hurricane. The large composites show similar behavior for the areas colder than −40° and −30°C contours. It is worth noting here that T_b around −40°C (i.e., homogeneous freezing of water) are typically the threshold for color enhancement of convective features in the tropics and are related to rainfall as summarized by Mapes and Houze (1993). However, the deepest convection and heaviest rain are better related to colder IR thresholds closer to −63°C (Liu et al. 2007). These composites suggest that R5 is better related to the IR patterns outside the TC core rather than those IR patterns closer to the core (i.e., those better related to intensity). Furthermore, these composites imply that R5 is related to the overall size of the cold T_b pattern including the convection-free moat region discussed in Frank (1977). This latter point appears to be the case particularly when comparing small- and average-sized composites where the relatively warm contours of −30°, −20°, and −10°C are nearly concentric, noting that these warmer contours extend outside the 600 km domain of our analysis in the large composites.

One interesting feature in the R5-based composites of major hurricanes is the suggestion that R5 is not well related to eye sizes, as measured by the radius maximum gradient of T_b (not shown). R5, however, is related to the width of the cold cloud ring surrounding the eye. Such differences would impact satellite-based intensity estimates made using the enhanced IR Dvorak technique (Dvorak 1984) where a minimum width of the coldest IR temperature ring surrounding the eye is a factor in determining TC intensity. Thicker cold cloud rings—those greater than 33–55 km depending on the temperature of the coldest surrounding T_b—would result in higher intensities, all other factors being the same. This finding suggests a potential cause of the Dvorak positive intensity biases associated with large major TCs (via the ROCI) reported in Knaff et al. (2010). It is noteworthy, however, that large TCs can have very large

eye features whereas the eye features in small storms are ultimately limited by the size of their convective core (e.g., as in Fig. 1). This eye size finding is a topic of future research.

Since the identification of TCs with intensities greater than or equal to 34 kt is less ambiguous[2] than weaker TCs and because more intense storms are of greater interest, the remainder of the paper will discuss results associated with TCs intensities (i.e., maximum wind speeds) of 34 kt or greater.

b. Interbasin distributions

Using the R5 metric we now investigate the TC size distributions as a function of TC basin. Figure 4 shows the frequency distribution of R5 in the North Atlantic, eastern North Pacific, western North Pacific, north Indian Ocean, and Southern Hemisphere TC basins as a function of storm intensity. Frequencies are again provided for tropical storm, minor hurricane, and major hurricane intensity samples. Table 3 contains the number of cases in each intensity range, along with the mean R5, standard deviation of R5, skew of R5, mean intensity, and mean latitude of each subsample. The differences of TC sizes between intrabasin intensity categories and between the different basins are also statistically significant at the 99% level based the sample sizes and the estimate of the population standard deviation (3.36) provided in Table 1. For instance, a mere difference of 0.36 in R5 with the smallest sample size (607 in the north Indian Ocean) is statistically significant at the 99% level.

Collectively, Fig. 4 and Table 3 indicate that TC size is a function of intensity with more intense TCs having larger average size distributions. Higher latitudes are also related to larger sizes (Table 3). The size distributions show that the eastern North Pacific (Fig. 4b) produces smaller tropical cyclones than all other basins. Sizes in that basin are about a third smaller than TCs in the North Atlantic (Fig. 4a) and western North Pacific (Fig. 4c), agreeing with R34-based findings in Knaff et al. (2007). The western North Pacific appears to generally have the largest most intense TCs, which agrees with conventional wisdom. Western North Pacific TCs are significantly larger than the TC sizes found in the North Atlantic despite the higher average latitudes of North Atlantic TCs. The 8% difference for major hurricanes compares nicely to results R34 based on Chan and Chan (2012). The north Indian Ocean TC basin (Fig. 4d) contains only a small fraction of the global TC activity. There are many more tropical storms in the north Indian Ocean record and the R5 distribution is noticeably different than the higher intensities. The few storms that become minor hurricanes produced a rather broad distribution of R5 with an indication of a bimodal nature. Most of the minor hurricanes appear to intensify to major hurricane strength as they move poleward (Table 3) and grow, shifting the R5 distributions to larger sizes while maintaining the general shape of the distribution. TCs in the Southern Hemisphere display R5 distributions (Fig. 4e) that are similar to those of the North Atlantic. However, unlike the TCs of the North Atlantic, TCs in this basin appear to develop and intensify in a rather narrow range of latitudes (Table 3). This suggests that the size distributions in this basin, while similar to the North Atlantic, may be caused by different mechanisms.

The standard deviations of R5 provide some indication of the variability of TC size in the various basins. The standard deviations of sizes of TCs appear to be largest in the North Atlantic and north Indian Ocean. The variations of minor hurricane sizes are largest in the north Indian Ocean followed by the Southern Hemisphere and North Atlantic. The variations of major hurricane sizes are largest in the Southern Hemisphere and eastern North Pacific but smallest in the western North Pacific. This latter finding suggest that in general the western North Pacific tends to produce large very intense storms whereas the Southern Hemisphere and east Pacific can produce relatively small and very intense cyclones. These findings will be reiterated when the spatial distribution of the largest and smallest TCs are discussed in section 4d.

The skew of the distributions, provided in Table 3, is also telling. To remind the readers, negative skew indicates that the tail on the left side of the probability density function is either longer or fatter than the right side, but it does not distinguish these shapes. Tropical storms (blue lines in Fig. 4) are negatively skewed in the western North Pacific and north Indian Ocean where as they are positively skewed in both the North Atlantic and eastern North Pacific. This suggests a possible tendency toward larger initial sizes in the western North Pacific and north Indian Ocean and toward smaller initial sizes in the Atlantic and eastern North Pacific. It is notable that, for minor hurricanes (the black lines in Fig. 4), the north Indian Ocean, western North Pacific, and Southern Hemisphere all have large negative skew or a tendency toward larger sizes. TC sizes of major hurricanes (the red lines in Fig. 4) are negatively skewed everywhere with the largest skew (tendency toward the

[2] The initiation of the best track is tied to the warning criteria of the warning agency. NHC and JTWC have different criteria for warnings and JTWC's warning criteria is dependent on the TC basin (NHC 2013; JTWC 2013). Knapp et al. (2013) shows how the length of TC lifetime and cumulative TC intensity statistics have been affected by changes in these criteria in the western North Pacific, particularly for TCs with maximum wind speed estimates less than 64 kt.

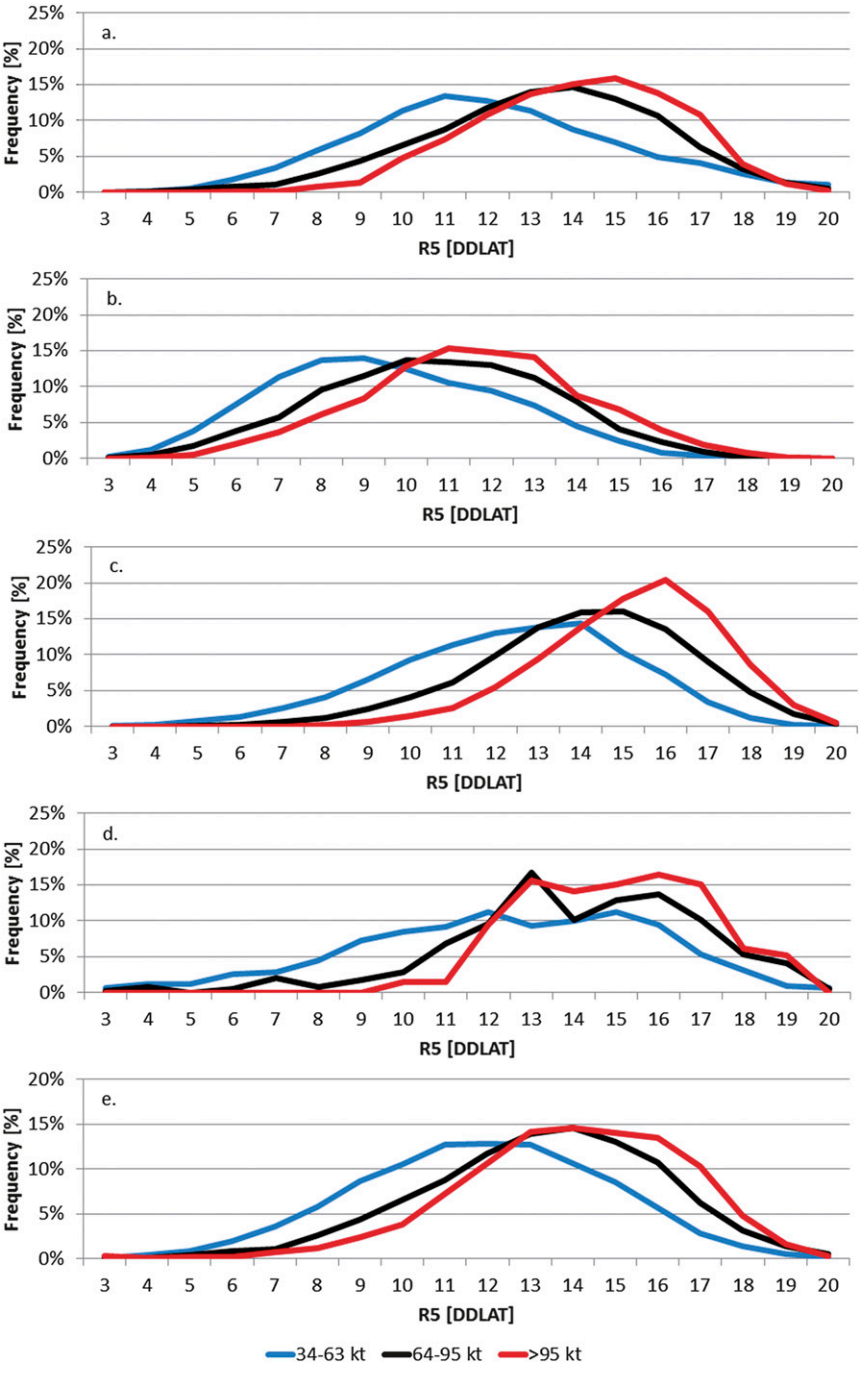

FIG. 4. Frequency distributions of TC size (R5) for the (a) North Atlantic, (b) eastern North Pacific, (c) western North Pacific, (d) north Indian Ocean, and (e) Southern Hemisphere tropical cyclone basins. Blue, black, and red lines are associated with tropical storm, minor hurricane, and major hurricane intensities as indicated in the key (see text for additional information). Units of R5 are distance in DDLAT.

large) occurring in the Southern Hemisphere, western North Pacific, and north Indian Ocean. Notable for this study is the tendency for a shift from a tendency of small weaker TCs to larger stronger TC in the North Atlantic and east Pacific. The skew becomes more negative with greater intensity in all basins save the north Indian Ocean, suggesting that TCs generally grow with intensification and higher latitudes.

TABLE 3. Statistics associated with Fig. 4. Shown are the intensity category, the number of cases, the mean R5, standard deviation σ and skew of R5, intensity V_{max}, and latitude. The units for R5 and V_{max} are DDLAT and knots, respectively.

Intensity category	Cases	R5	σ(R5)	Skew(R5)	V_{max}	Lat (°)
			North Atlantic			
Tropical storms	10 900	11.7	3.30	0.68	46.2	28.0
Minor hurricanes	4802	13.1	2.73	−0.09	76.3	28.2
Major hurricanes	1649	13.6	2.33	−0.21	115.1	22.1
			Eastern North Pacific			
Tropical storms	11 429	9.1	2.68	0.24	45.6	16.9
Minor hurricanes	5779	10.2	2.67	0.00	77.5	17.7
Major hurricanes	2790	11.1	2.57	−0.04	113.9	16.4
			Western North Pacific			
Tropical storms	17 141	11.8	2.75	−0.35	46.5	20.3
Minor hurricanes	9910	13.6	2.47	−0.38	78.0	21.4
Major hurricanes	5472	14.7	2.06	−0.50	117.4	19.6
			North Indian Ocean			
Tropical storms	2457	11.8	3.52	−0.47	43.8	14.3
Minor hurricanes	395	13.4	3.15	−1.01	75.4	15.7
Major hurricanes	212	14.5	2.06	−0.09	114.2	18.2
			Southern Hemisphere			
Tropical storms	18 178	11.4	2.89	−0.09	45.0	−17.3
Minor hurricanes	6857	12.8	2.74	−0.30	77.3	−17.6
Major hurricanes	3140	13.5	2.62	−0.63	112.4	−16.6

c. *TC growth life cycle*

In the previous section, the mean values of R5 indicate TCs generally grow, with those increases being related to changes in latitude and intensity. The shapes of the frequency distributions of minor and major hurricanes are generally negatively skewed, suggesting the intensification process results in a greater number of large TCs. In this section, we examine the life cycle of TC growth by stratifying the R5 statistic by the timing of the peak intensity, following Emanuel (2000), but we further stratify the composites by peak intensity ranges (e.g., tropical storm, minor hurricane, major hurricane). The first instance of maximum intensity is assigned to $t = 0$. Because of the small sample size in the north Indian Ocean TC basin (see Table 3), that basin is excluded from this analysis. Not only can we examine the life cycle of R5 but, since the latitude of each data point is known, we can examine the TC size changes that are not explicitly linked to latitude variation in the algorithm.

Figure 5 shows R5 (left) and the R5 metric with the latitude predictor in (1) removed (right) for the life cycle of tropical storms (top), minor hurricanes (middle), and major hurricanes (bottom) relative to the time of the first occurrence of the maximum lifetime intensity. Mean values are shown by the lines and standard error estimates are provided by the vertical bars. Concentrating on the left half of this figure a few observations can be made: 1) TCs tend to grow as they intensify; 2) if a TC is relatively large (small) in its formative stages, it likely will be relatively large (small) when it reaches maximum intensity; 3) the different basins seem to display both markedly different initial sizes and life cycle evolution, particularly for TCs that intensify into major hurricanes; and 4) TCs tend to shrink rapidly following peak intensity, save for in the North Atlantic.

When the influence of increasing latitude is not included in (1) (i.e., the right half of Fig. 5) there are several additional observations. First, the size of TCs in the eastern North Pacific and Atlantic are initially comparable but diverge after peak intensity. Second, there is some commonality between the size evolution of storms in the Southern Hemisphere and western North Pacific TCs. Tropical storms also do not grow much by factors other than those related to increasing latitude. This observation is also true for minor and major hurricanes in the eastern North Pacific and Southern Hemisphere. Much of the no-latitude-variational growth of minor hurricanes and major hurricanes in the western North Pacific occurs during and prior to maximum intensity, whereas the minor and major hurricanes in the Atlantic appear to continue to grow after maximum intensity is reached. This growth during weakening for Atlantic TCs has been documented in studies by Merrill (1984), Kimball and Mulekar (2004), and Maclay et al.

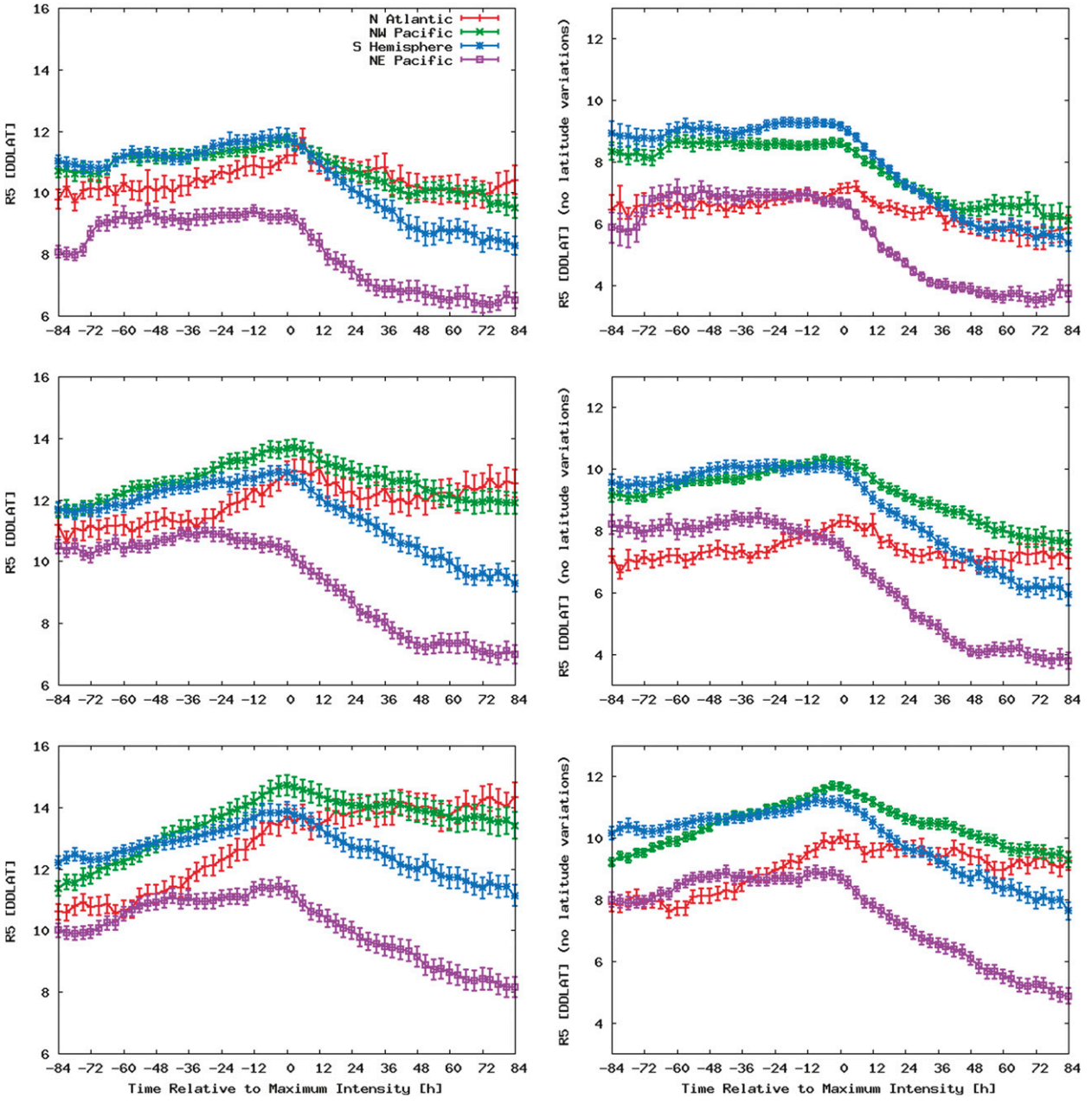

FIG. 5. Composites of TC size (R5) based on the timing of maximum intensity (i.e., time = 0 h): for TCs in the intensity V_{max} ranges (top) $34 \le V_{max} < 64$ kt, (middle) $64 \le V_{max} < 96$ kt, and (bottom) $V_{max} \ge 96$ kt of (left) R5 (right) R5 calculated without the latitude contribution. Vertical bars provide the standard error associated with each 3-hourly mean R5 value. The R5 units are in DDLAT.

(2008), but this study suggests that those findings cannot necessarily be extended to the other TC basins.

d. *Occurrence statistics of large and small TCs*

In this subsection we examine the occurrence statistics of large and small TCs as measured by R5. Here we concentrate on minor and major hurricanes, as these are more important from an energy perspective. Figure 6 shows the locations of the largest 25% and smallest 25% TCs at their first recorded maximum lifetime intensity. The statistics associated with the quartiles shown in Fig. 6 are provided in Table 4 and suggest that these quartiles are separated by 5–6 standard deviations and are statistically significant at the 99% level. The top panel of Fig. 6 shows the location of maximum intensity of minor hurricanes. The majority of the largest minor

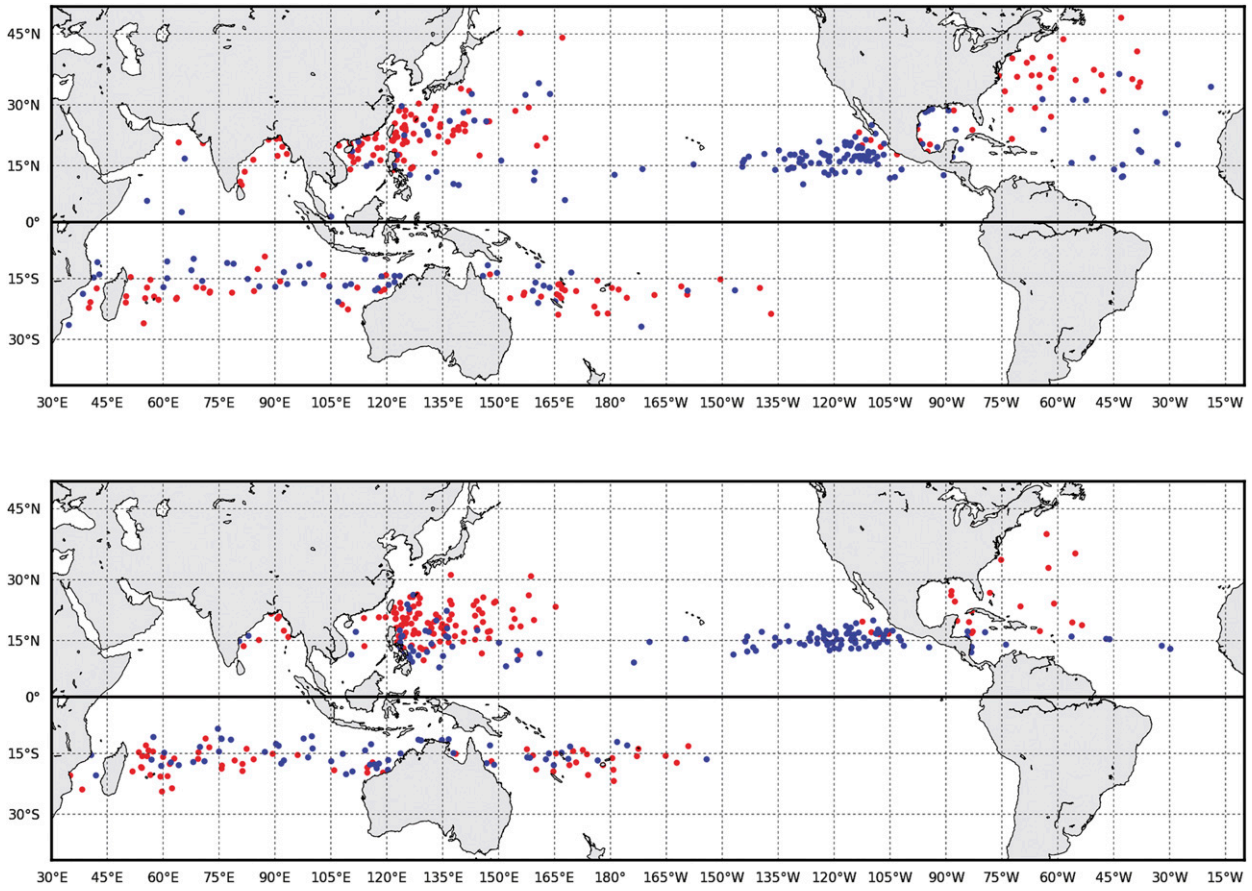

FIG. 6. Locations of the largest (red) and smallest (blue) 25% of TCs based according to R5. (top) TCs that reached minor hurricane intensity and (bottom) TCs that reached major hurricane intensity. Locations are based on the first maximum lifetime intensity.

hurricanes occur in the North Atlantic and western North Pacific in regions where TCs typically recurve [as shown in Fig. 1 of Knaff (2009)]. The majority of the small minor hurricanes occur in the eastern North Pacific and elsewhere either in the Northern Hemisphere subtropics or at low latitudes (equatorward of 20°). This later observation agrees with Brunt's (1969) statements suggesting that TCs at low latitudes tend to have small sizes. However, there is also evidence of a few small minor hurricanes occurring in the subtropical western North Pacific, which agrees well with the locations of midget typhoons–very small typhoons documented in Arakawa (1952), Brand (1972), and Harr et al. (1996). A similar subtropical occurrence of very small minor hurricanes occurs in the North Atlantic, which suggests that some very small hurricanes may form in similar environments as midget typhoons. Small and large minor hurricanes in the Southern Hemisphere are nearly equally distributed with larger storms, tending to occur at only slightly higher latitudes and again in regions where TCs more typically recurve. The Bay of Bengal has had a few large minor hurricanes, but given this basin's typical activity and vulnerability to storm surge this is noteworthy.

The bottom panel of Fig. 6 shows the location of maximum intensity of large and small major hurricanes. These results are similar to the location of maximum intensity of minor hurricanes but are generally shifted equatorward and are more concentrated in both the longitudinal and latitudinal directions, suggesting the importance of

TABLE 4. Statistics associated with the upper and lower quartiles of TC size (R5) for minor and major hurricane intensity TCs at the time of first maximum lifetime intensity shown in Fig. 6. The number of cases and the mean and the standard deviation σ associated with each quartile are listed. Means and standard deviations have units of DDLAT.

	Upper quartile (large)			Lower quartile (small)		
	No.	Mean	σ	No.	Mean	σ
Minor hurricanes	190	16.10	1.14	190	8.77	1.62
Major hurricanes	185	16.82	0.85	185	10.08	1.34

TABLE 5. Statistics associated with the basin-specific upper and lower quartiles of TC size (R5) for minor and major hurricane intensity TCs at the time of first maximum lifetime intensity shown in Fig. 7. The number of cases and the mean and the standard deviation σ associated with each quartile are provided. Means and standard deviations have units of DDLAT.

	Upper quartile (large)			Lower quartile (small)		
Intensity category	No.	Mean	σ	No.	Mean	σ
			North Atlantic			
Minor hurricanes	33	16.12	1.13	33	9.25	1.55
Major hurricanes	23	16.31	0.81	23	10.80	0.89
			Eastern North Pacific			
Minor hurricanes	39	13.62	0.95	39	6.88	1.23
Major hurricanes	40	14.36	2.03	40	8.15	1.10
			Western North Pacific			
Minor hurricanes	59	16.63	1.10	59	10.51	1.66
Major hurricanes	67	17.23	0.77	67	11.72	1.44
			Southern Hemisphere			
Minor hurricanes	53	16.05	0.91	53	9.37	1.55
Major hurricanes	51	17.06	0.77	51	10.45	1.84

warmer oceanic conditions for the strongest TCs (Riehl 1950; Michaels et al. 2006) and cooler tropical outflow temperatures (Emanuel 1986). Both the Bay of Bengal and Gulf of Mexico, known to be vulnerable to storm surge, can produce large major hurricanes. Large very intense TCs also seem to be more common near La Reunion in the southern Indian Ocean; Taiwan, Japan, the Philippines, and China in the western North Pacific and South Pacific; and the United States, the Bahamas, and Bermuda in the North Atlantic. The majority of small major hurricanes occur either in the eastern North Pacific or equatorward of 20° (i.e., very few in the subtropics). It is also noteworthy that equatorward of Australia small major hurricanes predominate.

Figure 6 shows where the largest and smallest TCs typically occur, but when the latitude influence is removed the distribution of small and large hurricanes does not appreciably change (not shown), which means that large TCs either begin as large storms (i.e., as implied in Fig. 5) and/or they continue to grow, following maximum intensity as is the case in the North Atlantic composites also shown in Fig. 5. Section 4e will discuss TC growth tendencies further.

Where large and small TCs typically exist is important, but when small and large TCs form is also interesting. Unlike Fig. 6, which shows global size quartiles, the results shown in Fig. 7 are based upon basin-specific quartiles, where large and small TCs are defined at the largest and smallest 25%, respectively. Table 5 provides the statistics associated with the basin-specific quartiles. Again the differences between small and large TC are statistically significant at the 99% level or greater.

Figures 7a,b show the monthly frequency distribution for small, large, and all minor hurricanes and major hurricanes in the North Atlantic, respectively. A 10% difference between the distributions is equivalent to a difference of 6.6 and 4.3 for minor and major hurricanes, respectively. Figure 7a indicates that small minor hurricanes begin earlier and peak later and have a little broader temporal distribution than large minor hurricanes. Figure 7b shows that larger major hurricanes have tended to occur earlier in the season, particularly in August, whereas small major hurricanes have had slightly higher frequencies in September and October. All and all the seasonality of TC size in North Atlantic is rather difficult to interpret without additional information and will be a topic of future studies.

Figures 7c,d shows the frequency distributions for small and large minor and major hurricanes in the eastern North Pacific. A 10% difference in this basin between the distributions is equivalent to a difference of 7.8 and 8.0 for minor and major hurricanes, respectively. In this basin, small minor hurricanes have occurred more frequently later in the season whereas large minor hurricanes are most frequent very early in the season. The frequency distribution of small major hurricanes peaks in July and small major hurricanes appear more frequent in May, June, and July. On the other hand, large major hurricanes in this basin occur later and are more frequent in August–December and small major hurricanes occur earlier (May–July). Again, these differences may be best related to other factors and could be a topic of future research.

In the western North Pacific, large and small minor hurricanes (Fig. 7e) have quite different frequency distributions. In these panels, a 10% difference between the distributions is equivalent to a difference of 11.8 and 13.4 for minor and major hurricanes, respectively.

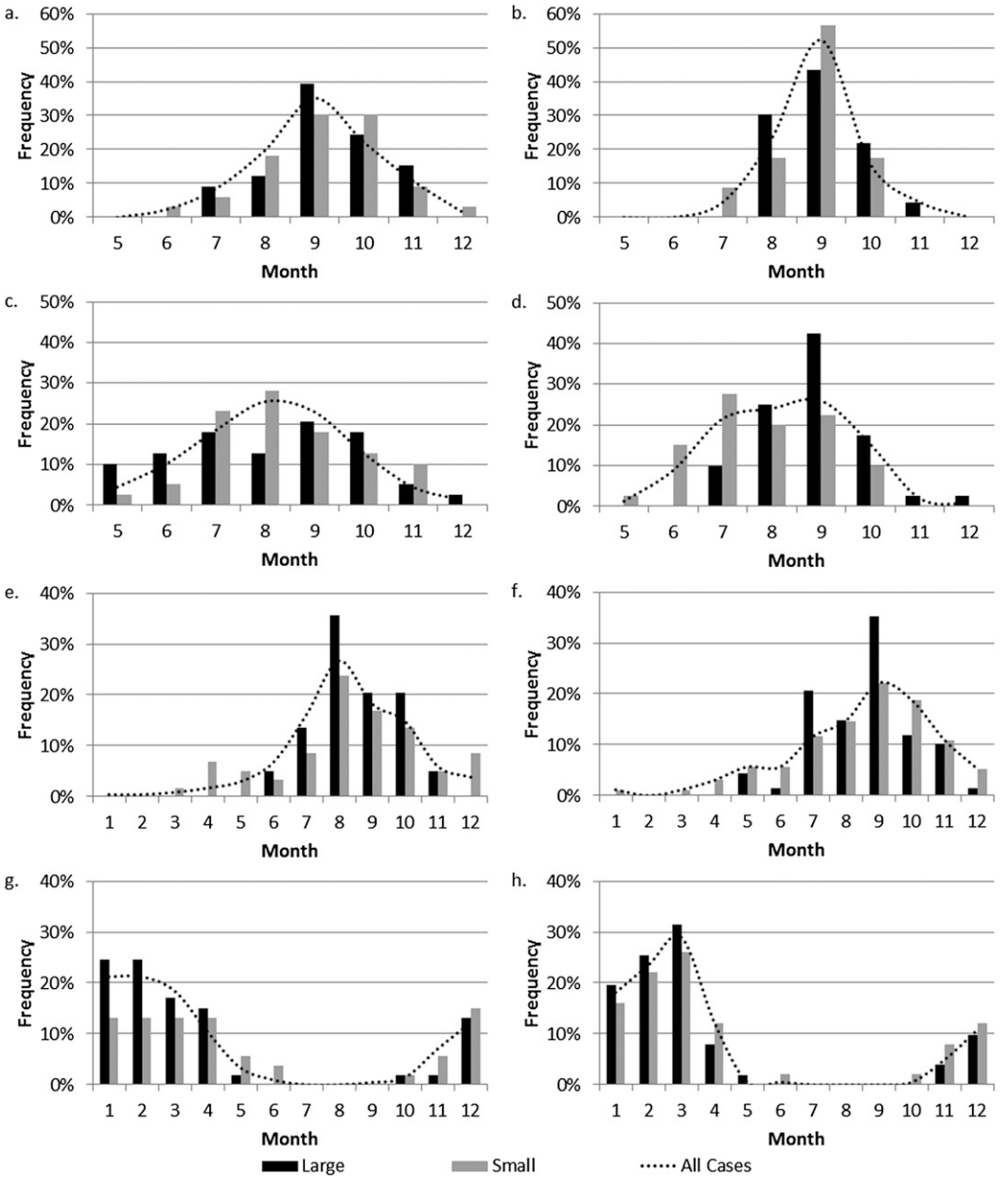

FIG. 7. Monthly frequency diagrams of TC size. Large (largest 25%) and small (smallest 25%) TC frequencies are shown along with the typical frequency of all storms. (left) Minor hurricanes and (right) major hurricanes. Results are based on the lower (small) and upper (large) quartiles in each basin. Results are from the (a),(b) North Atlantic, (c),(d) eastern North Pacific, (e),(f) western North Pacific, and (g),(h) Southern Hemisphere.

Large minor hurricanes in this basin have occurred more frequently than small minor hurricanes in the months of June–October and have a distribution that is more peaked and appears to be associated with the months when the equatorial southwesterly flow (i.e., monsoon trough) is most common. Small minor hurricanes occur more frequently than large minor hurricanes both before and after the peak of the season. Small major hurricanes (Fig. 7f) also occur more frequently before and after the normal peak of activity and were particularly more frequent in the months of October, November, December, January, April, and May. Large major hurricanes in this basin are most frequent in July, August, and September when low-level environmental vorticity is typically enhanced. These results agree well with findings presented in Brand (1972) and Lee et al. (2008).

The frequency of large and small TCs in the Southern Hemisphere (Figs. 7g,h) also seems to be related to seasonality of the equatorial northwesterly flow that episodically occurs in the southern Indian Ocean, north of Australia, and in the South Pacific convergence zone. In this basin, a 10% difference between the distributions is equivalent to a difference of 10.6 and 10.2 for minor and major hurricanes, respectively. Large minor and major hurricanes have been more common in the most active parts of the Southern Hemisphere TC season. Conversely, small minor and major hurricanes appear to be most common in both the early and late portions of the season in the months of October, November, March, April, and May. These again suggest that smaller TCs occur during times of suppressed low-level vorticity environments whereas large TCs tend to occur when low-level vorticity is generally enhanced.

Another aspect of the TC size climatology that is a topic of general interest is basin-specific listings of the largest and smallest major hurricane intensity TCs based on this algorithm. Table 6 provides basin-specific listings of the 10 largest and smallest major hurricane intensity TCs at their first time of maximum lifetime intensity. There are some notable names in these lists, but the reader should be aware that, while the earliest record for this study begins in 1978, data for many basins outside the North Atlantic and eastern North Pacific are often missing prior to 1981. There are a few interpretations that can be made from these lists, which provide potential topics for more thorough future investigation. In the Atlantic, the largest storms include several hurricanes that had minimum central pressures below 900 hPa and many of these also eventually made landfalls, with several in the Gulf of Mexico. In the eastern North Pacific, the majority of largest major hurricanes formed in years when the waters eastern equatorial Pacific was anomalously warm, whereas the small major hurricanes appear to predominate in years the eastern equatorial Pacific was anomalously cool or near average. The majority of largest major hurricanes in the western North Pacific formed in the months of July–mid-October and the smallest major hurricanes formed in the period mid-October–May. A similar finding holds in the Southern Hemisphere where the largest major hurricanes generally formed in December–February and the smallest major hurricanes formed in November, March, and April. Again this suggests the potential importance of the synoptic-scale vorticity environment to determining TC size.

e. Growth tendencies

Figure 8 (top panel) shows the tracks of the TCs that grow the fastest (top 10%) following maximum intensity and remain at least minor hurricanes. The most frequent regions for postpeak intensity TC growth are the regions to the east of the major continental landmasses of Asia, North America, Africa, and Australia. From the tracks shown in Fig. 8, these episodes of rapid postpeak intensity growth often occur in regions preferred for recurvature and extratropical transition. There is also some evidence that storms have the tendency to grow following landfall over narrow landmasses (e.g., the Philippines, Yucatan Peninsula, Florida), somewhat disagreeing with Brand and Blelloch (1973), who examined typhoon structure following landfall in the Philippines but only during the 24 h following reemergence in the South China Sea.

Figure 8 (middle) shows the tracks of TCs that decreased in size the most (top 10%) prior to attaining their maximum intensity and that remained hurricanes. These ''shrinking'' TC tracks are quite different than the postmaximum intensity TC growth cases, except for the North Atlantic, which shows similar tracks but fewer of them. The tracks of these shrinking TCs appear to be predominately associated with westward-moving nonrecurving TCs in the eastern North Pacific, western North Pacific, and southern Indian Ocean. However, the majority of these prepeak shrinking TCs that do recurve appear to have obtained maximum intensity following recurvature. Maximum intensity also typically occurs shortly after maximum size is obtained ($<$1 day). This result suggests that the synoptic-scale vorticity field, if negative like those the trade wind environment (i.e., westward-moving storms at low latitude), may not be able to support TC growth during intensification.

Figure 8 (bottom) shows the tracks associated with those hurricanes that reach both maximum intensity and size simultaneously. With the exception of the eastern North Pacific, hurricanes that display this behavior are characterized by landfall nearly coincident with maximum intensity, rather erratic tracks that suggest weak steering postrecurvature maximum intensity combined with poleward and eastward motion. Frequent landfalling cases in this category occurred in northern Australia, the South China Sea, the Gulf of Mexico, and the Bay of Bengal. The latter two track behaviors are often associated with less than ideal conditions for further intensification such as increased or constantly changing vertical wind shear, increased upper oceanic cooling associated with slow motion, and lower subtropical ocean heat contents (Knaff et al. 2013) and SSTs (Dare and McBride 2011). Erratic tracks in the subtropical regions also typically correspond to the TC being located within the subsidence region of the subtropical ridge that is typically characterized by subsidence, dryer mid- and upper-level environments, and negative environmental vorticity.

TABLE 6. A basin-specific list of the 10 largest and smallest major hurricanes at the time of first maximum lifetime intensity is shown. The storm name, date/time, maximum intensity V_{max}, and TC size R5 is provided. Units for V_{max} and R5 are knots and DDLAT, respectively.

Largest				Smallest			
Name	Date/time	V_{max}	R5	Name	Date/time	V_{max}	R5
North Atlantic							
Katrina	1800 UTC 28 Aug 2005	150	18.6	Frances	0000 UTC 9 Sep 1980	100	7.8
Gilbert	0000 UTC 14 Sep 1988	160	17.7	Beta	0600 UTC 30 Oct 2005	100	9.7
Opal	1200 UTC 4 Oct 1995	130	17.6	Felix	0300 UTC 3 Sep 2007	150	9.9
Ella	1200 UTC 4 Sep 1978	120	16.9	Bertha	2100 UTC 7 Jul 2008	109	10.2
Mitch	1800 UTC 26 Oct 1998	155	16.8	Eduardo	0700 UTC 25 Aug 1996	125	10.3
Alberto	1200 UTC 12 Aug 2000	110	16.8	Joan	0600 UTC 22 Oct 1988	125	10.4
Wilma	1200 UTC 19 Oct 2005	160	16.7	Alicia	0600 UTC 19830818/06	100	10.4
Rita	0600 UTC 22 Sep 2005	155	16.5	Fred	1200 UTC 9 Sep 2009	105	10.6
Gustav	2200 UTC 30 Aug 2008	130	16.3	Charlie	1800 UTC 13 Aug 2004	125	10.6
Gabrielle	0700 UTC 13 Sep 1989	135	16.1	Floyd	0000 UTC 7 Sep 1981	100	10.8
Eastern North Pacific							
Olivia	1800 UTC 21 Sep 1982	125	17.3	Felicia	0600 UTC 19 Jul 1997	115	5.1
Nora	1200 UTC 21 Sep 1997	115	16.7	Blanca	0000 UTC 14 Jun 1985	105	5.7
Lidia	0600 UTC 11 Sep 1993	130	16.3	Daniel	1800 UTC 30 Jun 1978	100	6.3
Norman	0000 UTC 3 Sep 1978	120	15.8	Barbara	1800 UTC 13 Jul 1995	120	6.5
Iniki	1800 UTC 11 Sep 1992	125	15.6	Ismael	1800 UTC 19 Aug 1989	105	6.6
Kiko	1800 UTC 3 Sep 1983	125	15.3	Lane	1800 UTC 6 Sep 1994	115	6.8
Herman	1200 UTC 1 Sep 2002	140	15.2	Jimena	1300 UTC 27 Aug 1997	115	7.1
Juliette	0600 UTC 25 Sep 2001	125	15.0	Lester	1200 UTC 22 Oct 1998	100	7.3
Guillermo	1800 UTC 4 Aug 1997	140	15.0	Dora	1800 UTC 16 Jul 1993	115	7.5
Rick	0600 UTC 18 Oct 2009	155	14.6	Hector	0600 UTC 3 Aug 1988	125	7.6
Western North Pacific							
Choi-Wan	0600 UTC 21 Sep 2003	100	19.7	Manny	1200 UTC 9 Dec 1993	120	7.3
Hagupit	1200 UTC 23 Sep 2008	125	19.6	Yunya	0600 UTC 14 Jun 1991	104	8.0
Oscar	0600 UTC 15 Sep 1995	140	18.9	Nari	1200 UTC 11 Sep 2001	100	8.0
Krosa	0000 UTC 5 Oct 2007	130	18.8	Yagi	1800 UTC 24 Oct 2000	105	8.7
Jangmi	0600 UTC 27 Sep 2008	140	18.7	Kujira	1800 UTC 4 May 2009	115	9.2
Nabi	1800 UTC 1 Sep 2005	140	18.4	Soulik	1800 UTC 3 Jan 2001	110	9.4
Man-Yi	0300 UTC 12 Jul 2007	125	18.2	Longwang	1200 UTC 28 Sep 2005	125	9.4
Tim	0600 UTC 10 Jul 1994	125	18.2	Meari	0600 UTC 24 Sep 2004	125	9.6
Haitang	1200 UTC 16 Jul 2005	140	18.1	Faye	0000 UTC 30 Oct 1985	100	9.7
Zeb	1200 UTC 13 Oct 1998	155	18.1	Neoguri	1800 UTC 17 Apr 2008	100	10.0
Southern Hemisphere							
Marlene	1800 UTC 3 Apr 1995	125	19.2	Bertie-Alvin	0000 UTC 23 Nov 2005	115	6.5
Ingrid	0000 UTC 28 Feb 1995	100	19.1	Nisha-Oram	1800 UTC 24 Feb 1983	97	6.8
Susan	0600 UTC 5 Jan 1998	140	18.5	Ned	1800 UTC 28 Mar 1989	100	7.5
Ofa	0600 UTC 4 Feb 1990	115	18.3	Agnes	0000 UTC 19 Apr 1995	110	7.8
Rhonda	0000 UTC 14 May 1997	100	18.2	Esau	1800 UTC 1 Mar 1992	115	8.3
Val	0000 UTC 8 Dec 1991	125	18.1	Oscar-Itseng	0000 UTC 26 Mar 2004	115	8.6
Gamede	1800 UTC 25 Feb 2007	105	18.0	Max	0600 UTC 15 Mar 1981	100	8.7
Anacelle	1200 UTC 11 Feb 1998	115	18.0	Ernest	0600 UTC 22 Jan 2005	100	9.0
Kerry	0000 UTC 17 Feb 1979	125	18.0	Billy	1800 UTC 24 Dec 2008	110	9.2
Jourdanne	0000 UTC 6 Apr 1993	125	17.9	Beni	1200 UTC 13 Nov 2003	100	9.2

f. Long-term trends in TC size

Since the combined effects of TC size and intensity (via increased kinetic energy) are related to hurricane damage potential (Powell and Reinhold 2007), upper ocean cooling (Knaff et al. 2013), and R34 (section 2), trends of TC size (R5) from our dataset are also examined. TC size trends were examined in two ways. We examined the TC size at maximum intensity and the maximum TC size for the combined sample of minor and major hurricanes (i.e., hurricanes collectively). The trend results of TC size at maximum intensity and at maximum size were nearly identical, reiterating the results in Fig. 4 that suggest the initial TC size is well

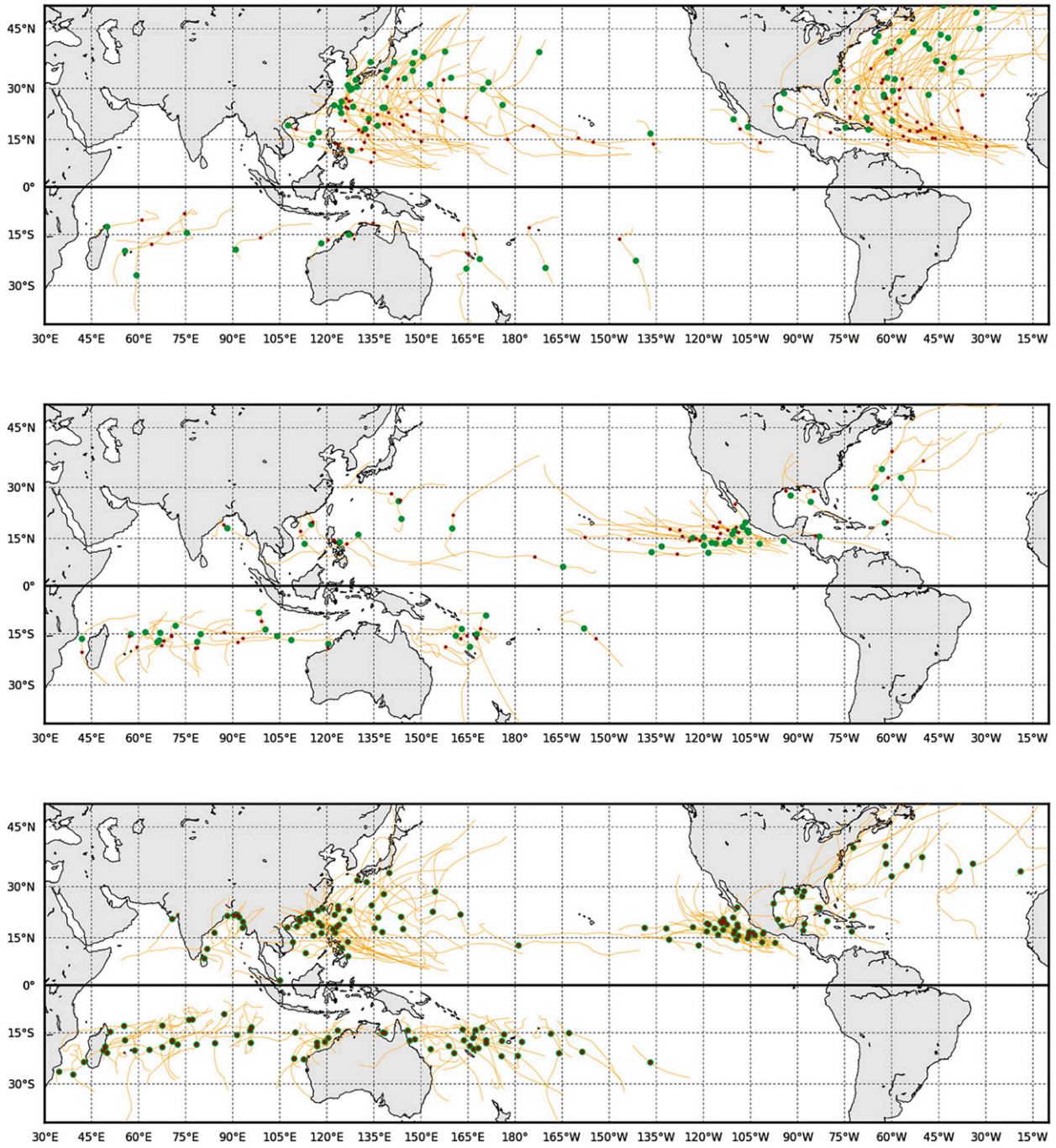

FIG. 8. Tracks associated with the hurricanes that displayed (top) the most rapid post maximum intensity growth and (middle) the most rapid decrease in size prior maximum intensity, and (bottom) those TCs that reached their maximum size and intensity simultaneously. The (top) and (middle) show the top 10% of the cases. The TC tracks (yellow), points of maximum intensity (maroon) and points where the hurricane is the largest (green) are shown. Results are based on cases 1978–2011.

related to the future size. For that reason, only the trends of maximum hurricane sizes are shown in Fig. 9. We also begin our TC size trend analysis in 1981, given that satellite data prior to that year are generally sparse in several TC basins.

Figure 9a shows the time series and trend of North Atlantic maximum hurricane size. The time series in the North Atlantic shows the R5 varies generally between values of 10° and 24° latitude, but the intra-annual variation is generally large producing a fairly consistent

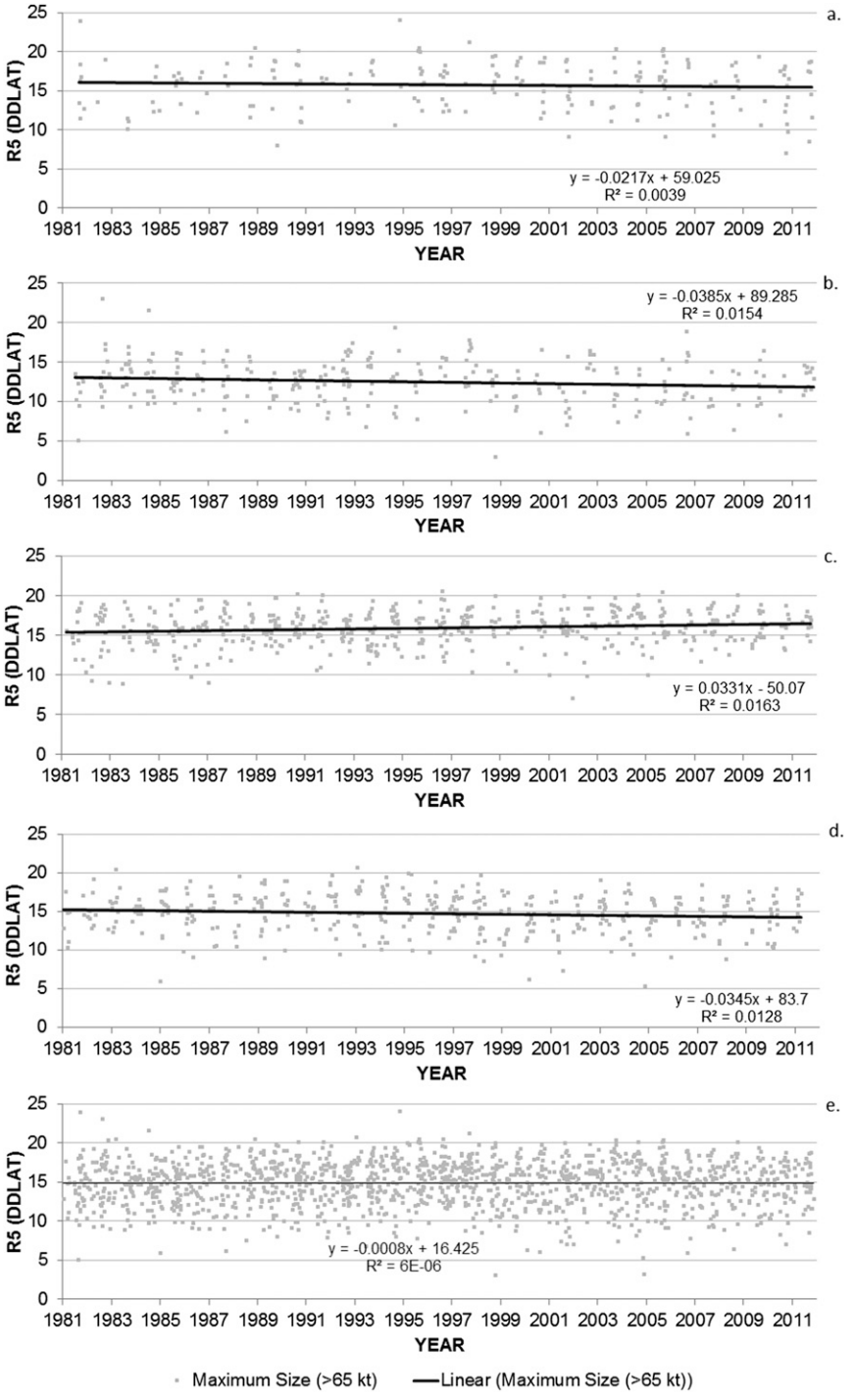

FIG. 9. Time series of TC size (R5) for the (a) North Atlantic, (b) eastern North Pacific, (c) western North Pacific, (d) Southern Hemisphere, and (e) global hurricanes (i.e., intensities > 63 kt) that occurred during the years 1981–2011 are shown. The individual TC values are shown along with a trend line (solid line). The regression equation and percent variance explained R^2 are also listed in each panel.

scatter between these ranges between 1981 and 2011. The resulting trends are slightly negative over these years and not statistically significant. Figure 9b shows the maximum hurricane size time series in the eastern North Pacific. The TC size variability in this basin is smaller, generally ranging between 6° and 17° latitude, with a few exceptions. As was the case in the North Atlantic, 1981–2011 trends are slightly negative and are not statistically significant. The time series of maximum hurricane size in the western North Pacific is shown in Fig. 9c. The maximum hurricane size in the western North Pacific varies roughly between 9° and 21° latitude. Trends of maximum hurricane size in this basin are slightly positive, but again are not statistically significant. Much like the western North Pacific, hurricane size in the Southern Hemisphere (Fig. 9d) is confined to a range of R5 with values generally between 9° and 21° latitude. The trends of TC size in the Southern Hemisphere are also found to be slightly negative, which again lack statistical significance. Finally, it is not surprising that the global trends of TC size of hurricane-strength TCs is essentially zero and lacking statistical significance, is dominated by storm-to-storm variability, and does not show any obvious signs of any clear relationship with known tropical interannual phenomenon. The reader is also directed toward Knutson et al. (2010) and references within for research related to current and future trends of TC intensity and precipitation.

5. Summary and discussion

The objective IR-based TC size metric R5 allows for an objective examination of the basic global TC size climatology including size distributions, typical evolutions, spatial distributions, seasonal tendencies, typical locations and tracks associated with growth and trends, and many other climatological–meteorological analyses. The basic climatological results presented here agree well with many of the results of past studies where ROCI and R34 were used as size metrics and concentrated on the North Atlantic and western North Pacific TC basins. We summarize our findings and discuss future research opportunities below.

Many of the findings of this study reconfirm past work in the North Atlantic and western North Pacific as discussed above but have put these in a global context. Results confirm that the propensity for large TCs increases when TCs form during seasons that are characterized by enhanced low-level vorticity and when TCs move into environments characterized as increasingly baroclinic, especially after peaking in intensity and prior to recurvature. This study confirms larger major hurricanes occur in the western North Pacific, which agrees with consensus. As others have shown, small TCs tend to form during seasons when low-level vorticity is provided by the incipient disturbance rather than the synoptic environment. In those cases the flow is often characterized by easterly trade winds or being located in the center of the subtropical ridge (as is often the case with midget typhoons). Postpeak intensity TC growth can also be halted by landfall and other rapid weakening.

However, a few new findings result from this study. Composites of the IR imagery indicate the average eye sizes are similar for small-, average-, and large-sized major hurricanes. In a global sense, there is a clear indication that small major hurricanes predominate at low latitudes. This study also allows for the direct comparison of size distributions between the individual TC basins and the identification of the smallest and largest major hurricanes in each of these basins. These summaries clearly show the differences between basins and confirms previous findings that the eastern North Pacific produces TCs that are about $^{2}/_{3}$ the size of other basins. We also find that there are preferred regions, seasons, and track types for TC sizes and growth tendencies. Information about the life cycle of TC growth with respect to the timing of maximum intensity is provided and leads to these findings:

1) TCs tend to grow more as they intensify.
2) If a TC is relatively large (small) in its formative stages, it likely will be relatively large (small) when it reaches maximum intensity.
3) Different basins display both markedly different initial sizes and life cycle size evolutions.
4) On average TCs shrink after peak intensity, save for in the North Atlantic.
5) The average North Atlantic major or minor hurricane maintains its size after peak intensity and stronger TCs continue to grow after peak intensity (suggesting results obtained from the Atlantic are not applicable everywhere).

Finally, the analysis of interannual trends of TCs with intensities greater than or equal to 64 kt show that between 1981 and 2011 there have been no significant trends in this objective measure of TC size.

There is much future work that can utilize the dataset produced by this approach, which can be maintained as long as there are TC best tracks and geostationary satellite data. These TC size estimates can be used to improve the understanding of what environmental factors—beyond generalizations of vertical wind shear, baroclinicity, etc.—are responsible for or related to TC growth. Such studies will make use of environmental diagnostics derived from numerical weather prediction analyses–reanalyses and other observational data. Such knowledge would

lead to the development of forecast techniques to better anticipate TC growth and allow the diagnosis of numerical model forecasts of TC growth. These datasets can also be applied to case studies of individual systems, especially those in the past, where traditional observations of TC size may be missing or uncertain. Finally, these data can be used for studies of the detailed interannual and intraseasonal variability of TCs. We look forward to working on a few of these problems in the near future.

Acknowledgments. The authors thank Mark DeMaria and Kate Musgrave for their insightful and constructive comments on initial versions of this manuscript, Julia Pillard for her manuscript preparation assistance, and Ken Knapp and the other anonymous reviewers for their constructive reviews. The views, opinions, and findings contained in this report are those of the authors and should not be construed as an official National Oceanic and Atmospheric Administration or U.S. government position, policy, or decision.

REFERENCES

Arakawa, H., 1952: Mame Taifu or midget typhoon (small storms of typhoon intensity). *Geophys. Mag.,* **24,** 463–474.

Brand, S., 1972: Very large and very small typhoons of the western North Pacific Ocean. *J. Meteor. Soc. Japan,* **50,** 332–341.

——, and J. W. Blelloch, 1973: Changes in the characteristics of typhoons crossing the Philippines. *J. Appl. Meteor.,* **12,** 104–109.

——, and C. P. Guard, 1979: An observational study of extratropical storms evolved from tropical cyclones in the western North Pacific. *J. Meteor. Soc. Japan,* **57,** 479–482.

Brunt, A. T., 1969: Low latitude cyclones. *Aust. Meteor. Mag.,* **17,** 67–90.

Chan, K. T. F., and J. C. L. Chan, 2012: Size and strength of tropical cyclones as inferred from QuikSCAT data. *Mon. Wea. Rev.,* **140,** 811–824.

Chavas, D. R., and K. A. Emanuel, 2010: A QuikSCAT climatology of tropical cyclone size. *Geophys. Res. Lett.,* **37,** L18816, doi:10.1029/2010GL044558.

Cocks, S. B., 1997: The outer radius tangential winds of tropical cyclones. M.S. thesis, Dept. of Atmospheric Science, Colorado State University, 102 pp. [Available from Morgan Library, Colorado State University, Fort Collins, CO 80523.]

——, and W. M. Gray, 2002: Variability of the outer wind profiles of western North Pacific typhoons: Classifications and techniques for analysis and forecasting. *Mon. Wea. Rev.,* **130,** 1989–2005.

Dare, R. A., and J. L. McBride, 2011: Sea surface temperature response to tropical cyclones. *Mon. Wea. Rev.,* **139,** 3798–3808.

Dean, L., K. A. Emanuel, and D. R. Chavas, 2009: On the size distribution of Atlantic tropical cyclones. *Geophys. Res. Lett.,* **36,** L14803, doi:10.1029/2009GL039051.

DeMaria, M., 2009: A simplified dynamical system for tropical cyclone intensity prediction. *Mon. Wea. Rev.,* **137,** 68–82.

——, M. Mainelli, L. K. Shay, J. A. Knaff, and J. Kaplan, 2005: Further improvement to the Statistical Hurricane Intensity Prediction Scheme (SHIPS). *Wea. Forecasting,* **20,** 531–543.

Demuth, J., M. DeMaria, and J. A. Knaff, 2006: Improvement of Advanced Microwave Sounding Unit tropical cyclone intensity and size estimation algorithms. *J. Appl. Meteor. Climatol.,* **45,** 1573–1581.

Depperman, C. E., 1947: Notes on the origin and structure of Philippine typhoons. *Bull. Amer. Meteor. Soc.,* **28,** 399–404.

Dvorak, V. F., 1984: Tropical cyclone intensity analysis using satellite data. NOAA Tech. Rep. 11, 45 pp. [Available from NOAA Central Library, 1315 East-West Highway, SSMC3, 2nd Floor, Silver Spring, MD 20910.]

Emanuel, K. A., 1986: An air-sea interaction theory for tropical cyclones. Part I: Steady-state maintenance. *J. Atmos. Sci.,* **43,** 585–605.

——, 2000: A statistical analysis of hurricane intensity. *Mon. Wea. Rev.,* **128,** 1139–1152.

——, 2010: Tropical cyclone activity downscaled from NOAA-CIRES reanalysis, 1908–1958. *J. Adv. Model. Earth Syst.,* **2** (1), doi:10.3894/JAMES.2010.2.1.

Evans, C., and R. E. Hart, 2008: Analysis of the wind field evolution associated with the extratropical transition of Bonnie (1998). *Mon. Wea. Rev.,* **136,** 2047–2065.

Frank, W. M., 1977: The structure and energetics of the tropical cyclone I. Storm structure. *Mon. Wea. Rev.,* **105,** 1119–1135.

Harr, P. A., M. S. Kalafsky, and R. L. Elsberry, 1996: Environmental conditions prior to formation of a midget tropical cyclone during TCM-93. *Mon. Wea. Rev.,* **124,** 1693–1710.

Holland, G. J., 1980: An analytic model of wind and pressure profiles in hurricanes. *Mon. Wea. Rev.,* **106,** 1212–1218.

Houston, S. H., W. A. Shaffer, M. D. Powell, and J. Chen, 1999: Comparisons of HRD and SLOSH surface wind fields in hurricanes: Implications for storm surge and wave modeling. *Wea. Forecasting,* **14,** 671–686.

Irish, J. L., D. T. Resio, and J. J. Ratcliff, 2008: The influence of storm size on hurricane surge. *J. Phys. Oceanogr.,* **38,** 2003–2013.

JTWC, cited 2013: Frequently asked questions. Naval Oceanography Portal. [Available online at http://jtwccdn.appspot.com/JTWC/frequently-asked-questions-1/frequently-asked-questions.]

Kalnay, E., and Coauthors, 1996: The NCEP/NCAR 40-Year Reanalysis Project. *Bull. Amer. Meteor. Soc.,* **77,** 437–471.

Kaplan, J., M. DeMaria, and J. A. Knaff, 2010: A revised tropical cyclone rapid intensification index for the Atlantic and east Pacific basins. *Wea. Forecasting,* **25,** 220–241.

Kidder, S. Q., J. A. Knaff, S. J. Kusselson, M. Turk, R. R. Ferraro, and R. J. Kuligowski, 2005: The tropical rainfall potential (TRaP) technique. Part I: Description and examples. *Wea. Forecasting,* **20,** 456–464.

Kimball, S. K., and M. S. Mulekar, 2004: A 15-year climatology of North Atlantic tropical cyclones. Part I: Size parameters. *J. Climate,* **17,** 3555–3575.

Knaff, J. A., 2009: Revisiting the maximum intensity of recurving tropical cyclones. *Int. J. Climatol.,* **29,** 827–837.

——, and R. M. Zehr, 2007: Reexamination of tropical cyclone wind–pressure relationships. *Wea. Forecasting,* **22,** 71–88.

——, C. R. Sampson, M. DeMaria, T. P. Marchok, J. M. Gross, and C. J. McAdie, 2007: Statistical tropical cyclone wind radii prediction using climatology and persistence. *Wea. Forecasting,* **22,** 781–791.

——, D. P. Brown, J. Courtney, G. M. Gallina, and J. L. Beven II, 2010: An evaluation of Dvorak technique-based tropical cyclone intensity estimates. *Wea. Forecasting,* **25,** 1362–1379.

——, M. DeMaria, D. A. Molenar, C. R. Sampson, and M. G. Seybold, 2011: An automated, objective, multisatellite platform

tropical cyclone surface wind analysis. *J. Appl. Meteor. Climatol.,* **50,** 2149–2166.

——, ——, C. R. Sampson, J. E. Peak, J. Cummings, and W. H. Schubert, 2013: Upper oceanic energy response to tropical cyclone passage. *J. Climate,* **26,** 2631–2650.

Knapp, K. R., and J. P. Kossin, 2007: New global tropical cyclone data from ISCCP B1 geostationary satellite observations. *J. Appl. Remote Sens.,* **1,** 013505, doi:10.1117/1.2712816.

——, M. C. Kruk, D. H. Levinson, H. J. Diamond, and C. J. Neumann, 2010: The International Best Track Archive for Climate Stewardship (IBTrACS): Unifying tropical cyclone best track data. *Bull. Amer. Meteor. Soc.,* **91,** 363–376.

——, J. A. Knaff, C. R. Sampson, G. Riggio, and A. Schnapp, 2013: A pressure-based analysis of the historical western North Pacific tropical cyclone intensity record. *Mon. Wea. Rev.,* **141,** 2611–2631.

Knutson, T. R., and Coauthors, 2010: Tropical cyclones and climate change. *Nat. Geosci.,* **3,** 157–163, doi:10.1038/ngeo779.

Kossin, J. P., J. A. Knaff, H. I. Berger, D. C. Herndon, T. A. Cram, C. S. Velden, R. J. Murnane, and J. D. Hawkins, 2007: Estimating hurricane wind structure in the absence of aircraft reconnaissance. *Wea. Forecasting,* **22,** 89–101.

Lee, C.-S., K. K. W. Cheung, J. S. N. Hui, and R. L. Elsberry, 2008: Mesoscale features associated with tropical cyclone formations in the western North Pacific. *Mon. Wea. Rev.,* **136,** 2006–2022.

——, ——, W.-T. Fang, and R. L. Elsberry, 2010: Initial maintenance of tropical cyclone size in the western North Pacific. *Mon. Wea. Rev.,* **138,** 3207–3223.

Liu, C., E. J. Zipser, and S. W. Nesbitt, 2007: Global distribution of tropical deep convection: Different perspectives from TRMM infrared and radar data. *J. Climate,* **20,** 489–503.

Maclay, K. S., M. DeMaria, and T. H. Vonder Haar, 2008: Tropical cyclone inner core kinetic energy evolution. *Mon. Wea. Rev.,* **136,** 4882–4898.

Mapes, B. E., and R. A. Houze Jr., 1993: Cloud clusters and superclusters over the oceanic warm pool. *Mon. Wea. Rev.,* **121,** 1398–1416.

Matyas, C. J., 2010: Associations between the size of hurricane rain fields at landfall and their surrounding environments. *Meteor. Atmos. Phys.,* **106,** 135–148.

Merrill, R. T., 1984: A comparison of large and small tropical cyclones. *Mon. Wea. Rev.,* **112,** 1408–1418.

Michaels, P. J., P. C. Knappenberger, and R. E. Davis, 2006: Sea-surface temperatures and tropical cyclones in the Atlantic basin. *Geophys. Res. Lett.,* **33,** L09708, doi:10.1029/2006GL025757.

Mueller, K. J., M. DeMaria, J. A. Knaff, J. P. Kossin, and T. H. Vonder Haar, 2006: Objective estimation of tropical cyclone wind structure from infrared satellite data. *Wea. Forecasting,* **21,** 990–1005.

NHC, cited 2013: Glossary of NHC terms. [Available online at http://www.nhc.noaa.gov/aboutgloss.shtml#TROPCYC.]

Powell, M. D., and T. A. Reinhold, 2007: Tropical cyclone destructive potential by integrated kinetic energy. *Bull. Amer. Meteor. Soc.,* **88,** 513–526.

Riehl, H., 1950: A model of hurricane formation. *J. Appl. Phys.,* **21,** 917–925.

Sampson, C. R., and A. J. Schrader, 2000: The automated tropical cyclone forecasting system (version 3.2). *Bull. Amer. Meteor. Soc.,* **81,** 1231–1240.

Schumacher, A. B., M. DeMaria, and J. A. Knaff, 2009: Objective estimation of the 24-hour probability of tropical cyclone formation. *Wea. Forecasting,* **24,** 456–471.

Shoemaker, D. N., 1989: Relationships between tropical cyclone deep convection and the radial extent of damaging winds. University of Colorado Department of Atmospheric Science Paper 457, 109 pp. [Available from Morgan Library, Colorado State University, Fort Collins, CO 80523.]

Weatherford, C. L., and W. M. Gray, 1988: Typhoon structure as revealed by aircraft reconnaissance. Part II: Structural variability. *Mon. Wea. Rev.,* **116,** 1044–1056.

Zehr, R. M., and J. A. Knaff, 2007: Atlantic major hurricanes, 1995–2005—Characteristics based on best track, aircraft, and IR images. *J. Climate,* **20,** 5865–5888.